Scale Effect on Porosity and Permeability: Kinetics, Model, and Correlation

Faruk Civan
Mewbourne School of Petroleum and Geological Engineering, The University of Oklahoma, Norman, OK 73019

Variation of porosity and permeability by scale dissolution and precipitation in porous media is described based on fractal attributes of the pores, realization of flow channels as a bundle of uniformly distributed mean-size cylindrical and tortuous hydraulic flow tubes, a permeability-porosity relationship conforming to Civan's power law flow units equation, and the pore surface scale precipitation and dissolution kinetics. Practical analytical solutions, considering the conditions of typical laboratory core tests and relating the lumped and phenomenological parameters, were derived and verified by experimental data. Deviations of the empirically determined exponents of the pore-to-matrix volume ratio compared to the Kozeny-Carman equation were due to the relative fractal dimensions of pore attributes of random porous media. The formulations provide useful insights into the mechanism of porosity and permeability variation by surface processes and accurate representation of the effect of scale on porosity and permeability by simpler lumped-parameter models.

Introduction

Processes involving porous media are encountered in the nature and various engineering systems. Therefore, characterization of porous materials, including their porosity and permeability relationship, is an interdisciplinary subject. In spite of many experimental and theoretical studies of the permeability of porous materials, a satisfactory model still does not exist for prediction and/or correlation of permeability of porous materials undergoing alteration by contact with pore fluids.

Interactions of pore fluids with porous matrix frequently cause scale problems in porous materials. Scale formation or removal from pore surface by precipitation or dissolution of certain substances during flow of solutions through porous media frequently cause a variation of pore volume and pore surface, and therefore porosity and permeability, which affect the rate of the various porous media transport processes. In subsurface reservoirs, the porosity and permeability vary by the natural dissolution and precipitation of solids, such as minerals and salts during flow of aqueous phase, asphaltene and paraffin during flow of crude oil, and sulfur during flow of natural gas. In various engineering systems involving porous materials, induced precipitation or dissolution of various scales over pore surface may occur. Therefore, prediction of the variation of the characteristics of porous materials due to scales is an important problem for accurate modeling of transport in porous materials.

Nelson (1994) carried out a parametric analysis of the available permeability-porosity models developed for stationary porous formations. Ordinarily, these models are not intended for applications for porous formations undergoing alteration of formation properties by rock-fluid interactions. However, some have been modified to account for porous media alteration leading to dynamic permeability-porosity relationships. As emphasized by Nelson (2000), engineers desire to predict permeability from porosity, but other factors including types of clays, grain size, composition, and deformation, creation of noncontributing porosity by rock-fluid interactions, and pore jamming and cementing by various substances, may also effect the permeability of porous formations in a complicated manner. Nelson (2000) stresses that "there is no initial dependence between permeability and porosity in newly deposited sands. It is only through diagenetic processes that an apparent dependence or correlation develops between permeability and porosity."

Rajani (1988), Panda and Lake (1994), and Le Gallo et al. (1998) classified the approaches to representing the permeability-porosity relationship into two categories based on the flow realization as follows: (1) Flow-through a bundle of hy-

draulic tubes of porous media and (2) flow-around the grains of porous media. Le Gallo et al. (1998) compared the available models of the both types and concluded that neither were satisfactory in describing the permeability-porosity relationship in porous media undergoing alteration by rock-fluid interactions for the considered test problems.

Reis and Acock (1994) investigated the accuracy of a variety of models proposed for prediction and/or correlation of permeability vs. porosity reduction by precipitation of inorganic solids in porous media. They evaluated the exponential, power law, straight and sinusoidal capillary tubes, the Kozeny-Carman (Kozeny, 1927; Carman, 1937, 1938, 1956), and statistical network models. The best results were obtained by the sinusoidal capillary tubes model, because the "constriction factor" considered in this model could be adjusted for best representation of the experimental data. This model attempts to simulate the pore throat narrowing and/or jamming phenomena, referred to as the "gate or valve effect" by Chang and Civan (1997) and Ochi and Vernoux (1998). However, Figure 6 of Reis and Acock (1994) indicates that even the sinusoidal tubes model could not accurately represent the experimental data. The Reis and Acock (1994) study has exclusively demonstrated that these models do not satisfactorily represent the experimental data. There are other important factors. For example, Liu and Civan (1996) and van der Marck (1999) consider a nonzero-transport threshold, and Revil and Cathles III (1999) consider the cementation effects.

Civan (2000a) provides a critical review of the presently available models for describing the porosity and permeability of porous materials, and their relationships. He grouped these models into three categories: empirical equations, hydraulic tube models, and network models. The empirical models are obtained by correlation of the porosity and permeability data obtained by testing of porous materials with specific fluids. Empirical correlations, which are not based on theory, do not provide an insight into the mechanism of the porosity and permeability alteration processes, and they are applicable only over the range of experimental data used to develop them. Extrapolation of their use to conditions beyond the range of data may be misleading. Artificial neural networks can also be classified as empirical models, because they need the tuning and training of a multiparameter empirical equation by adjusting its parameters using experimental data. The porous media network models are instructive and informative, because they allow insight into the internal details of the porous media flow and they are important research and development tools. However, they are impractical to use for routine engineering simulation and design tasks due to the required exhaustive computational effort. Further, the network models frequently assume certain pore body and pore throat realizations, which may only approximate actual porous structure to a certain level of sophistication. Saito et al. (1995) caution that selecting pore models with certain regularities may be insufficient, because the arrangement of porous media grains and void spaces can also strongly affect the permeability. Hydraulic tube models are a reasonable compromise between the empirical and network models. Hydraulic tube models consider a bundle of tortuous flow tubes analogy of the paths followed by the fluid flowing through a porous material. These models assume that the Hagen-Poiseuille hydraulic tube flow and the Darcy porous media flow models represent the flow across porous materials equally well, there is no cross-flow among the flow tubes formed between the inlet and outlet sides of porous materials, and the flow tube diameter is uniform along the flow path. Coupling the Hagen-Poiseuille, Darcy, and the mean-hydraulic tube diameter concept leads to the Kozeny-Carman model (Kozeny, 1927; Carman, 1937, 1938, 1956), which has been extensively used in the literature for wide range of applications. This model has been popular because it is simple and practical, and it provides a logical insight into the physics of flow through porous media and the effective parameters, such as porosity, permeability, tortuosity, and specific surface. Although it provides a relationship between the relevant parameters, the Kozeny-Carman model is still classified as a semi-analytical model, because some of these parameters must be measured and/or correlated empirically. Saito et al. (1995) point out that this model contains an empirical parameter, the value of which depends on the configuration of the pore structure. Saito et al. (1995) determined that permeability strongly depends on porosity and the arrangement of the porous matrix and pore space, and, hence, the pore-size distribution. As far as the effect of the fluid is concerned, the majority of the reported work assumed that fluids flowing through porous media were single-phase and behaved Newtonian. Honma (1993) considered non-Newtonian fluids of various types and derived Kozeny-Carman type single-phase non-Newtonian permeability-porosity models. The modeling problem would be further complicated when the effects of multiphase fluid systems and different flow regimes, such as non-Darcian vs. Darcian, were to be considered.

In order to minimize the effort in developing empirical correlations guided by the Kozeny-Carman hydraulic tubes model, Amaefule et al. (1993) rearranged the equation to express the mean-hydraulic tube diameter proportionally to the pore volume to porous matrix volume ration, as follows, referred to as the linear flow units equation by Civan (2000a)

$$\sqrt{\frac{K}{\phi}} = \gamma\left(\frac{\phi}{1-\phi}\right) \tag{1}$$

where K and ϕ denote the permeability and porosity of porous media. Consequently, the tortuosity and specific grain surface parameters, and the constant have been conveniently combined into one group, reducing the number of empirical parameters to be determined to one combined parameter, as

$$\gamma = \left(\Sigma_g\sqrt{2\tau}\right)^{-1} \tag{2}$$

where Σ_g is the specific grain surface and τ is the tortuosity. Amaefule et al. (1993) named this group as a flow-zone indicator. Here, it is referred to as a flow-unit parameter. Thus, different porous materials can be classified into and identified as specific flow-units, whose parametric relationships according to Eq. 1 have distinct values of the flow-unit parameter values. As a result, different regions of heterogeneous porous media having different property values could be identified in terms of the same flow-unit parameter values. This approach provides significant convenience in the characteri-

zation of highly heterogeneous porous media, and great advantage by reducing the complexity of the modeling and the computational effort necessary to simulate transport phenomena in heterogeneous porous media.

Although the flow-units approach taken by Amaefule et al. (1993) provides a practical means of circumventing the difficulties dealing with local heterogeneities in porous media, its applicability and accuracy are limited by the inherent simplifying assumptions of the Kozeny-Carman hydraulic tube model; after all, Amaefule et al. (1993) simply rearranged this equation for convenience in the determination of the flow-units parameter. The outstanding limitation of this model is due to the assumption that the flow tubes remain open or conductive at all times because of the definition of hydraulic tubes and the use of this concept for realization of porous media. Further, this equation can only provide a first-order approximation to the relation between the mean tube diameter and the pore to solid volume ration, that is, the relationship given by Eq. 1 is linear. Therefore, this model is primarily intended for applications to static porous materials, whose effective or conductive pore structure (fabric, texture, morphology, and so on) and properties (porosity, permeability, tortuosity, specific surface, and so on) remain unchanged during fluid flow. Hence, this model does not allow for the alteration of porous media by interactions of fluids with porous matrix.

Civan (1996, 2000b) alleviated the shortcomings of the Kozeny-Carman equation in a practical manner by incorporating the gate effect for porous media undergoing alteration by an interactive process between pore fluids and porous matrix. Civan (1996) modified the Amaefule et al. (1993) equation (Eq. 1), by expressing the mean-hydraulic tube diameter as a power law function of the pore volume-to-solid volume ration as follows, referred to as the Civan power-law flow units equation

$$\sqrt{\frac{K}{\phi}} = \gamma\left(\frac{\phi}{1-\phi}\right)^{\beta} \tag{3}$$

where γ and β are empirically determined parameters. Civan (1996, 2000a) proposed and verified this equation based on the analyses of the trends in experimental data. Civan (2000b) has shown that these parameters could be correlated as functions of the coordination number Z representing the number of pore throats emanating from a pore body. For all practical purposes, this implies that the values of these parameters remain constant provided that the coordination number does not change during porous media alteration. As the comparisons of the model and experimental data presented by Civan (2000b) and in this article attest, this is a valid assumption for the dissolution and precipitation processes, which primarily occur at the pore surface (Le Gallo et al., 1998). However, when porous media alteration primarily occurs by pore throat plugging, such as during flow of suspension of fine particles through porous media, this assumption is no longer valid, and other appropriate treaties should be considered to determine the dependency of these parameters to the variation of the coordination number, as well as other relevant parameters, including the rate coefficient for pore throat plugging. Then, the process is significantly complicated, because the flow is diverted to other open channels as pore throats in certain flow paths are being plugged by the deposits. This process is not considered here, because Gruesbeck and Collins (1982), Liu and Civan (1996), and Civan (2000a) have adequately formulated the porosity and permeability variation by fine particles deposition in porous media. These models consider the "gate or valve effect" (Ohen and Civan, 1993, Chang and Civan, 1997; Ochi and Vernoux, 1998) of the pore throats. As pore throats are plugged by solid precipitate, the pores are isolated from each other and the permeability rapidly diminishes. Gruesbeck and Collins (1982) referred to this phenomenon as the "snow-ball effect". Under these circumstances, the permeability may even attain a zero value, but the noncontributing, and thus total, porosity may not necessarily be zero. Therefore, Eq. 1 based on open tortuous hydraulic tubes model cannot simulate this phenomenon.

Correlation of a variety of experimental data according to Eq. 3 has indicated that the values of these parameters are strong functions of the coordination number (Civan, 2000a,b), and may be significantly different than and $\gamma = (\Sigma_g\sqrt{2\tau})^{-1}$ and $\beta = 1$ implied by the Kozeny-Carman Eq. 1. For example, Civan (2000b) obtained correlations of Rajani's (1988) experimental data of permeability and porosity with coefficients of regression of the least-squares linear fit of data very close to one using Eq. 3, indicating that Eq. 3 accurately represents these data. The best estimates of the parameters were obtained to be $\gamma = 4.1$ and $\beta = 2.96$ for one type of porous rock, and $\gamma = 5.82$ and $\beta = 3.89$ for another. Civan (2000b) has determined that the experimental data by Ridgway and Tarbuck (1967) and the data generated using a network model by Bhat and Kovscek (1999) could be correlated using the γ and β parameters as functions of the coordination number by

$$|1-\gamma/\gamma_\infty| = |1-(\phi/\phi_\infty)^{\zeta}| = \exp(-\tilde{A}Z+\tilde{B}) \tag{4}$$

$$|1-\beta^{-1}/\beta_\infty^{-1}| = \exp(-\tilde{C}Z+\tilde{D}) \tag{5}$$

with least-squares coefficients of regressions very close to one, indicating that Eqs. 4 and 5 accurately represent the functional dependency of these parameters on the coordination number Z. $\tilde{A}$, $\tilde{B}$, $\tilde{C}$, $\tilde{D}$, and ζ are empirical parameters. ϕ_∞, γ_∞, and β_∞ denote the ϕ, γ, and β-parameter values at the limit as Z approaches infinity. The absolute values were used in Eqs. 4 and 5 because γ and β^{-1} increase for dissolution and decrease for precipitation. For example, the Ridgway and Tarbuck (1967) dissolution data could be accurately represented by (Civan, 2000b)

$$\gamma/\gamma_\infty = (\phi/\phi_\infty)^{18} = 1+\exp(-2.218Z+26.69) \tag{6}$$

The β parameter was not correlated for the Ridgway and Tarbuck (1967) data, because they did not measure the necessary permeability versus porosity data. However, Civan (2000b) correlated the Bhat and Kovscek (1999) simulated precipitation data accurately by

$$\gamma/\gamma_\infty = 1-\exp(-0.2567Z+0.4883) \tag{7}$$

$$\beta^{-1}/\beta_\infty^{-1} = 1-\exp(-0.1915Z+0.1320) \tag{8}$$

These exercises have confirmed the validity of the empirical Eqs. 3–5. Equation 3 is further confirmed by analyzing additional data in the present study. Further, the validity of Eq. 3 is also theoretically proven for the first time based on the fractal hydraulic tubes model in this article.

Extensive reviews of dynamic processes and mathematical models involving the interactions of pore fluids and porous matrix and leading to scale deposition/dissolution, as well as porosity and permeability alteration are available by Civan (2000a) and Magnico (2000). Description of dynamic reaction-transport in reactive porous media requires kinetic equations for representation of the rate of dissolution/precipitation of inorganic and organic scales to determine the amount of dissolution or precipitation and the resulting alteration of the porous media characteristics. Steefel and Lasaga (1990), Ortoleva (1994) and Holstad (1995) presented similar rate expressions to represent the dissolution and precipitation-induced porosity variation. The validity and empirical parameters of these expressions have been determined by matching of the reaction-transport models to experimental data (Liu et al., 1997). The effect of scale formation or dissolution at the pore surface on the permeability of porous media has been investigated by several researchers, including Schechter and Gidley (1969) and Glover and Guin (1973), who developed mathematically complicated models based on the realization of porous media as a bundle of randomly distributed capillary tubes with a population, varying by surface reaction. Comparisons of their model predictions with experimental data have indicated that these models have inherent disadvantages despite the intricate details considered in the construction of these models. First, the solution of the resulting nonlinear integro-differential equation derived in these studies requires tedious numerical treatment with inherent numerical errors. Second, direct interpretation and correlation of experimental data with these equations are not possible, because the solution of these models requires numerical techniques. Third, these models do not accurately represent the experimental data. For example, judging by the results presented in Figures 4 and 5 by Glover and Guin (1973), the quality of the predictions degenerates rapidly at later times. Under these conditions, apparently the complicated mathematical modeling does not pay off and therefore is not justifiable.

Magnico (2000) developed a Lagrangian model and obtained semi-analytical solutions for clogging in a one-dimensional porous medium. Instead of using the empirical Kozeny-Carman equation, Magnico (2000) represented the interstitial pore space in porous media by a capillary tube analogy so that the cross-sectional area of the capillary flow tube represents the permeability of porous media according to the Darcy law. Magnico (2000) assumed that deposition of precipitates essentially occurs over the pore surface by empirically determined n-th order precipitation reaction, which in turn changes the cross-sectional area of the flow tube and therefore the permeability of porous media. Although the theoretical exercise presented by Magnico (2000) is instructive and provides useful insight into the porous media clogging process, the resulting semi-analytical expressions are still significantly complicated for practical applications and have not been validated by experimental data.

It is apparent from the above discussion that further studies are necessary towards developing better permeability-porosity models. The work presented in this article facilitates pore description by fractals to improve the hydraulic tubes model considering a Darcian flow of a single-phase, incompressible, and Newtonian fluid through porous media. The theoretical derivation of the Civan power-law flow units equation (Civan, 1996, 2000a) (Eq. 3) for permeability-porosity relationship is given for the first time in this article. The present study develops still a simplified model for permeability and porosity of porous media undergoing alteration by scale precipitation or dissolution. The resulting model equations consist of a differential rate equation for dissolution/precipitation and an algebraic equation representing the porosity and permeability relationship. Under the variable conditions of pore fluids and porous media, they should be solved numerically. Because the model is simple, the numerical solution scheme can be incorporated into complicated porous media reaction-transport models without an appreciable computational burden. However, under the simplifying conditions of the laboratory tests considered here, such as constant rate rapid flow, single-phase, incompressible, and Newtonian fluid, constant solute concentration, and constant temperature, the rate expressions can be analytically integrated and the resultant relationships can be simplified under certain conditions, as demonstrated in the following section, for convenience in the comparison of the model with data. This leads to the development of lumped-parameter models. These expressions are then verified by means of a variety of data involving porosity and permeability variation by scale precipitation/dissolution in porous media. This confirms that the simplified lumped-parameter models developed in this article accurately represent the experimental data. In addition, the values of the lumped parameters are determined in each case.

The modeling approach taken in this study is guided by the philosophy of J. Willard Gibbs, who appropriately expressed that "The purpose of a theory is to find that viewpoint from which experimental observations appear to fit the pattern" (Duda, 1990). In turn, when an appropriate theory can be found for a given process, it may provide some insight into the nature of things, that is, the mechanisms and parameters of the governing process, as demonstrated by the present study.

Formulation

Figure 1 shows the irregular pore structure in a representative elementary bulk volume of a porous material. The representative elementary volume is an optimum bulk size of porous media over which the microscopic properties of pore fluids and porous matrix can be averaged to obtain a consistent and continuous macroscopic description. Brown et al. (2000) define it as "the range of volumes for which all averaged geometrical characteristics are single-valued functions of the location of that point and time." As pointed out by Nelson (2000), the total porosity of porous formations can be classified into the contributing and noncontributing porosities. The interconnected pore space allowing flow through constitutes the contributing porosity. The remaining pore space, physically isolated, forms the noncontributing porosity. However, some connected pores may be trapped within dead or stationary fluid regions and therefore may not be able to contribute to flow under prescribed flow conditions. This is

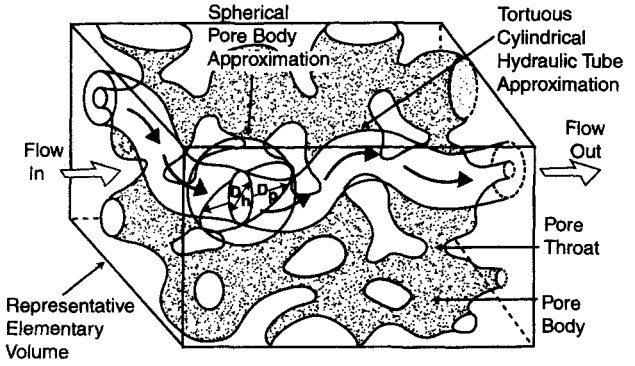

Figure 1. Spherical shape pore body and cylindrical shape tortuous hydraulic tube approximation in a representative elementary volume of a porous medium.

another permeability effecting factor, dependent on the prevailing flow conditions. As pointed by Nelson (2000), the porosity term appearing in the Kozeny-Carman equation refers to the contributing or effective porosity. Frequently, for convenience in modeling, pore structure in porous media is viewed as a collection of pore bodies connected with pore throats, as shown in Figure 1, which are referred to as the nodes and bonds, respectively, in the network models. The number of the pore throats emanating from a pore body to surrounding pore bodies is a characteristic parameter and, denoted by Z, called the coordination number. Its average value over the representative elementary volume for a prescribed pore structure is uniquely defined.

As described by Civan (2000a), alteration in porous media occurs when immobile deposits are formed within the pore space. The flow characteristics are determined by several factors, including coordination number, mean-pore diameter, mean-hydraulic tube diameter, specific pore surface, and tortuosity. When a suspension of particles flows through porous media, particles may deposit over the pore surface and/or accumulate behind the pore throats, as depicted in Figure 2, when the conditions are favorable for deposition. Pore throat

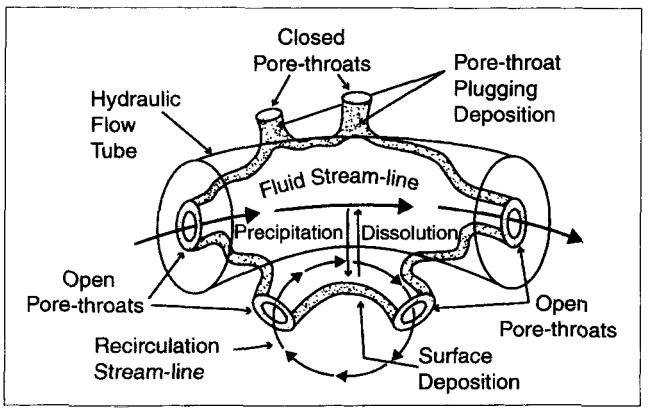

Figure 2. Surface deposition and pore-throat plugging deposition involving a pore body and associated pore throats.

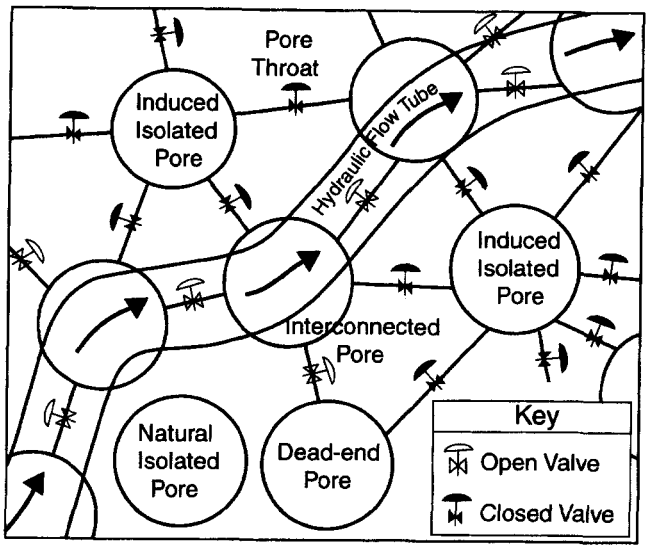

Figure 3. Valve effects of pore throats in a network of pore bodies connected with pore throats in a porous medium.

plugging primarily occurs by particulates suspended in the fluid and causes severe permeability damage, because the plugs formed by jamming of the pore throats, which act like valves, constrict and/or limit the through flow. When the pore throats are plugged, the interconnectivity of pores are reduced, some pores may in fact become dead-end pores or isolated pores as shown in Figure 3. Consequently, the permeability of porous media diminish to zero when a sufficient number of pore throats are closed to interrupt the continuity of the flow channels. Therefore, during the alteration of porous media, the fluid paths continuously vary, adopting to the least resistant paths available under the prevailing conditions. Whereas, dissolution and precipitation processes in porous media most likely occur at the pore surface (Le Gallo et al., 1998), which is in abundance availability in porous materials. As depicted in Figure 2, dissolution and precipitation processes result in scale removal and scale formation at the pore surface, respectively. Therefore, for the most part, it is reasonable to assume that pore throat plugging phenomenon can be neglected, except at the limit when the pore throat opening is significantly reduced by surface deposition to an extent that it can exert a sufficient resistance to prevent flow through the pore throat. Thus, for all practical purposes, it is reasonable to assume that the coordination number remains unchanged during the surface dissolution and precipitation processes, and, hence, the parameters of the Civan power law flow units Eq. 3 can be considered constant values under these conditions, as demonstrated with various data in the applications section.

The alteration of the flow paths, as described above, can only be determined by means of the network modeling. Although more instructive, such internally detailed elaborate description of flow in an intricately complicated and varying porous structure may be cumbersome and computationally demanding, and, therefore, is not warranted for most practical problems. Frequently, simplified models, such as developed here, based on a lumped-parameter representation of

the processes over the representative elementary bulk volume of porous media, are sufficient and, in fact, preferred. The lumped parameter model developed here assumes that a hydraulic flow tube or a preferential flow path is formed by interconnecting the pore bodies, like beads on a string, as described in Figures 1 and 3. Consequently, the pore body and pore throat diameters are averaged as the mean-hydraulic tube diameter. The coordination number and tortuosity are assumed to remain constant during dissolution and precipitation, because the pore throat plugging effect is negligible. The rate of variation of the pore volume is assumed directly proportional to the instantaneous available pore volume and the participating pore surface, over which scale can be formed because of the affinity of the precipitating substance to the substrate present at the pore surface. In addition, fractal relationships are facilitated, with the fractal parameters determined empirically, to describe the various geometrical attributes of the flow paths in random porous media. Ultimately, the fractal coefficients and dimensions are incorporated into the lumped parameters. The validity of these assumptions are verified in the applications section, where it is demonstrated that the equations derived based on these assumptions can accurately represent the typical experimental data.

Let A_h, P_h and L_h denote the cross-sectional area, perimeter, and length of the mean hydraulic flow tube. n denotes the number of hydraulic tubes providing flow through porous media. Then, the bulk volume of porous medium and the pore volume of all the hydraulic tubes V_p in a bulk representative elementary volume V_b of porous media are given respectively by

$$V_b = A_b L_b \tag{9}$$

$$V_p = nA_h L_h = V_b \phi \tag{10}$$

The tortuosity τ of the mean hydraulic tube is defined as the ration of the hydraulic tube length L_h to the bulk length L_b of porous media by

$$\tau = L_h / L_b \tag{11}$$

Thus, from Eqs. 9–11

$$\phi = \tau n A_h / A_b \tag{12}$$

The total pore surface of all the hydraulic tubes are given by the fractal relationship as

$$\Sigma_p = nP_h L_h = \mathfrak{C}(V_b \Sigma_b)^{\mathfrak{D}/3} = \mathfrak{C}\left[V_b \Sigma_g (1-\phi)\right]^{\mathfrak{D}/3} \tag{13}$$

where $\mathfrak{C}$ is a fractal coefficient and $\mathfrak{D}$ is a fractal dimension. For $\mathfrak{C} = 1$ and $\mathfrak{D} = 3$, Eq. 13 simplifies to the following conventional expression

$$\Sigma_p = nP_h L_h = V_b \Sigma_b = V_b \Sigma_g (1-\phi) \tag{14}$$

where Σ_b and Σ_g denote the total pore surface per unit bulk volume and total pore surface of hydraulic tubes per unit matrix grain volume, respectively. Equations 10 and 13 yield

$$nP_h \tau L_b = \mathfrak{C}\left[nA_h \tau L_b \Sigma_g (1-\phi)/\phi\right]^{\mathfrak{D}/3} \tag{15}$$

For $\mathfrak{C} = 1$ and $\mathfrak{D} = 3$, Eq. 15 simplifies to the following conventional expression

$$\frac{A_h}{P_h} = \frac{1}{\Sigma_g}\left(\frac{\phi}{1-\phi}\right) \tag{16}$$

A fractal relationship is considered between the pore surface area and the pore volume of the mean-hydraulic tube, inferred by Johns and Gladden (2000), as follows:

$$\Sigma_p / n = C(V_p/n)^{D/3} \tag{17}$$

where C and D are empirical fractal coefficient and fractal dimension, respectively. They can be determined by the intercept and slope of a straightline fit of the pore surface vs. pore volume data on a log-log scale, similar to the procedure applied by Johns and Gladden (2000). In porous materials, pore surface is frequently measured by adsorption and the pore volume is determined by injection of mercury or an environmentally friendly fluid. As stated by Johns and Gladden (2000), the value of the fractal dimension D vary between the Euclidean dimension of $D = 2$ and the embedding dimension of $D = 3$. Consequently, the fractal dimension can be viewed as a measure of the pore surface roughness. Johns and Gladden (2000) demonstrated the determinability of the fractal dimension for dissolution of globes from the slope of the best straight-line fit of the experimental data with an expression similar to Eq. 17 on the logarithmic scale. They found that the fractal dimension is about $D = 2.3$, very close to the Euclidean dimension of $D = 2$ for the system tested in their study. Substituting Eqs. 10, 11, and 14 into Eq. 17 yields

$$P_h = C(L_b \tau)^{-1+D/3} A_h^{D/3} \tag{18}$$

Invoking Eq. 18 into Eq. 16 yields the following expression for the cross-sectional area of a flow tube

$$A_h = \frac{1}{L_b \tau}\left(\frac{C}{\mathfrak{C}}\right)^{3/(\mathfrak{D}-D)} \Sigma_g^{-\mathfrak{D}/(\mathfrak{D}-D)} n^{(3-\mathfrak{D})/(\mathfrak{D}-D)} \times \left(\frac{\phi}{1-\phi}\right)^{\mathfrak{D}/(\mathfrak{D}-D)} \tag{19}$$

For $\mathfrak{C} = 1$ and $\mathfrak{D} = 3$, Eq. 19 simplifies to the following expression

$$A_h = \frac{1}{L_b \tau}\left(\frac{C}{\Sigma_g}\right)^{1/(1-D/3)} \left(\frac{\phi}{1-\phi}\right)^{1/(D/3)} \tag{20}$$

Next, consider the flow of an incompressible and Newtonian single-phase fluid through porous media. The Darcy law

represents the rate of volumetric flow through porous media

$$q = \frac{KA_b}{\mu}\frac{\Delta p}{L_b} \tag{21}$$

Alternatively, based on a bundle of hydraulic tubes realization of porous media flow channels, the Hagen-Poiseuille equation can be facilitated, given by:

$$q = n\frac{\pi D_h^4}{128\mu}\frac{\Delta p}{L_h} \tag{22}$$

A_b is the surface area of the bulk porous media normal to flow including the pores open for flow and the porous matrix not permitting flow through, given by

$$A_b = nA_h + A_m \tag{23}$$

where A_m denotes the cross-sectional area of the matrix normal to flow.

The hydraulic tube diameter is given by (De Nevers, 1970)

$$D_h = 4A_h/P_h \tag{24}$$

The cross-sectional area open for flow, that is, the areosity of porous media, is given by the fractal relationship

$$A_f = A_b c\phi^{d/3} = nA_h \tag{25}$$

where c is a fractal coefficient and d is a fractal dimension. Previous studies used $c = 1$ and $d = 3$. However, Liu and Masliyah (1996) recommend $d = 2$. However, these parameters should be determined empirically for given porous media. For $c = 1$ and $d = 3$, Eq. 25 simplifies to the following conventional expression

$$A_f = A_b\phi = nA_h$$

The cross-sectional area of a hydraulic tube is given by

$$A_h = \pi D_h^2/4 \tag{27}$$

Consequently, equating Eqs. 21 and 22, and then substituting Eqs.11 and 24–27 leads to the following expression for the mean hydraulic tube diameter

$$D_h = 2\sqrt{\frac{A_h}{\pi}} = 4\sqrt{\frac{2\tau}{c}}\sqrt{\frac{K}{\phi}}\,\phi^{-(1/2)(d/3-1)} \tag{28}$$

which simplifies to the following conventional expression for $c = 1$ and $d = 3$

$$D_h = 2\sqrt{\frac{A_h}{\pi}} = 4\sqrt{2\tau}\sqrt{\frac{K}{\phi}} \tag{29}$$

Substituting Eq. 20 into Eq. 28 leads to

$$\sqrt{\frac{K}{\phi}} = \gamma\phi^{\upsilon}\left(\frac{\phi}{1-\phi}\right)^{\beta} \tag{30}$$

where

$$\beta = \frac{1}{2(1-D/\mathfrak{D})} \tag{31}$$

$$\gamma = \frac{n^{(1/2)(3-\mathfrak{D})/(\mathfrak{D}-D)}(C/\mathfrak{C})^{3/(2(\mathfrak{D}-D))}}{2\tau\sqrt{2\pi L_b/c}} \tag{32}$$

$$\upsilon = \frac{1}{2}\left(\frac{d}{3}-1\right) \tag{33}$$

For $c = 1$, $d = 3$, Eq. 30 simplifies to Civan's (1996, 2000a,b) power-law flow units equation

$$\sqrt{\frac{K}{\phi}} = \gamma\left(\frac{\phi}{1-\phi}\right)^{\beta} \tag{34}$$

in which

$$\beta = \frac{1}{2(1-D/\mathfrak{D})} \tag{35}$$

$$\gamma = \frac{n^{(1/2)(3-\mathfrak{D})/(\mathfrak{D}-D)}(C/\mathfrak{C})^{3/(2\mathfrak{D}-D))}}{2\tau\sqrt{2\pi L_b}} \tag{36}$$

This theoretical derivation is a proof of the validity of Civan's (1996) equation, (Eq. 3) which was derived empirically. Equations 35 and 36 also express the empirical parameters in terms of the physically meaningful parameters. As can be seen by this exercise, the exponent is different than $\beta = 1$ implied by the Kozeny-Carman equation (Eq. 1).

For convenience, Eqs. 3 or 34 can be written in a scaled form as follows, by applying them at a reference state, denoted by the subscript o, and at any state, without a subscript, and then dividing the resulting expressions side-by-side- to obtain

$$\frac{K\phi_o}{K_o\phi} = f(\beta,\gamma)\left[\frac{\phi(1-\phi_o)}{\phi_o(1-\phi)}\right]^{2\beta} \tag{37}$$

in which

$$f(\beta,\gamma) = \left(\frac{\gamma}{\gamma_o}\right)^2\left(\frac{\phi_o}{1-\phi_o}\right)^{2(\beta-\beta_o)} \tag{38}$$

where K_o and ϕ_o denote the reference porosity and permeability values. As demonstrated in the applications section using Bertero et al. (1988) data, Eq. 37 can be plotted as a straight-line on the logarithmic scale once the beta and

gamma values approach constant terminal values, denoted as β_∞ and γ_∞, respectively. Therefore, Eq. 38 assumes a constant value, denoted by f_∞.

Describing the hydraulic flow tube diameter by the fractal concept, the new expressions given by Eqs. 35 and 36 were obtained for the β and γ parameters of Eq. 34. These are different than the values indicated by the Kozeny-Carman Eq. 1. In the applications section, the values of the β and γ parameters are obtained by the least-squares linear regression of Eq. 37 to experimental dissolution/precipitation-induced porosity and permeability variation data, for which $f = f_\infty$.

Following Walsh et al. (1982) and Lichtner (1992), a mineral dissolution (backward) or precipitation (forward) reaction, such as the gypsum and quartz precipitation reactions given by Carnahan (1990)

$$Ca^{2+}_{(aq)} + SO^{2-}_{4(aq)} + 2H_2O \leftrightarrow CaSO_4 \cdot 2H_2O_{(s)} \tag{39}$$

$$Si(OH)^{o}_{4(aq)} \leftrightarrow SiO_{2(s)} + 2H_2O \tag{40}$$

can be represented in general by (Liu et. al., 1997)

$$M + \sum_{i=1}^{N} \nu_i S_i = 0 \tag{41}$$

where M denotes a mineral $S_i: i = 1, 2, \ldots, N$ represent the number of aqueous species associated with the mineral reaction, and υ_i are some stoichiometric coefficients, which are positive for the products and negative for the reactants. The actual ion activity product for Eq. 41 is given by

$$K_{ap} = \prod_{i=1}^{N} a_{i,\text{actual}}^{\upsilon_i} \tag{42}$$

where a_i is the activity of species i. The equilibrium saturation ion activity product is given by

$$K_{sp} = \prod_{i=1}^{N} a_{i,\text{equilibrium}}^{\upsilon_i} \tag{43}$$

Hence, the saturation ration can be defined as (Oddo and Tomson, 1994)

$$F_s = K_{ap}/K_{sp} \tag{44}$$

The rate of pore volume variation by dissolution/precipitation of a solid in porous media is directly related to several driving forces and/or factors (Steefel and Lasaga, 1990; Ortoleva, 1994; Holstad, 1995; and Civan, 1996): (1) deviation of the saturation ratio F_s from unity ($F_s < 1$, $F_s = 1$, and $F_s > 1$ indicate undersaturation, equilibrium, and supersaturation, respectively; (2) volume of pore fluid (for precipitation, the volume of fluid is equal to the instantaneous pore volume, which is the initial pore volume minus the volume of the precipitating deposits; for dissolution, it is equal to the initial pore volume plus the volume of dissolving deposits); and (3) pore surface available and having affinity for dissolution/precipitation. Hence, a rate equation for porosity variation by dissolution/precipitation can be written as:

$$-dV_p/dt = k(F_s - 1)V_p\Sigma_p^m \tag{45}$$

where k is a dissolution/precipitation rate coefficient, m is an exponent of pore surface participation, and t is time. Note that only the pore surface having affinity to scale forming precipitate is considered. Thus, substituting Eqs. 10 and 17 into Eq. 45 yields the following rate equation for porosity variation by scale

$$-d\phi/dt = k_\phi \phi^{1+r} \tag{46}$$

where

$$r = mD/3 \tag{47}$$

$$k_\phi = k(F_s - 1)C^m n^{m-r} V_b^r \tag{48}$$

The initial porosity is given by

$$\phi = \phi_o, t = 0 \tag{49}$$

When the saturation ratio F_s varies at actual pore fluid conditions, Eqs. 46–49 should be numerically integrated along with the reaction-transport equations to consider the effect of varying saturation ratio of the solution. However, when the saturation ratio is maintained constant, such as the case with the specially designed laboratory tests conducted to generate the experimental data used in the applications section, the solution of Eqs. 46–49 can be obtained analytically as follows

For $m = 0$,

$$\phi/\phi_o = \exp(-k_\phi t) \tag{50}$$

and for $m \neq 0$,

$$\phi^{-r} - \phi_o^{-r} = k_\phi t \tag{51}$$

which can be rearranged as

$$\phi/\phi_o = (1 + k_\phi \phi_o^r t)^{-1/r} \tag{52}$$

These analytical solutions are convenient and useful for analyzing and interpreting precipitation/dissolution-induced porosity and permeability variation data obtained under constant saturation conditions. They can also be used to determine the lumped dissolution/precipitation rate coefficient k_ϕ and the lumped r parameter under given saturation conditions, that is, when F_s is constant.

Although the above derivation primarily focused on the porosity variation ($d\phi/dt$), an analogous equation can be readily derived for the rate of solid dissolution/precipitation ($d\epsilon_s/dt$) by expressing the porosity of the inert porous matrix ϕ_o as a sum of the instantaneous porosity ϕ and the fractional bulk volume ϵ_s occupied by dissolving/precipitating solid or scales as

$$\phi_o = \phi + \epsilon_s \tag{53}$$

If σ denotes the scale volume expressed as the occupied fraction of the original pore volume fraction ϕ_o, then it follows that

$$\epsilon_s = \phi_o \sigma \tag{54}$$

Thus, invoking Eq. 54 into Eq. 53, the instantaneous porosity is given by

$$\phi = \phi_o(1-\sigma) \tag{55}$$

Equation 55 is used in the applications section for analyzing Bertero et al. (1988) data.

Substituting Eq. 50 for $m = 0$ into Eq. 37 yields

$$\frac{K}{K_o} = e^{-\alpha t}\left[\frac{1-\phi_o}{1-\phi_o e^{-k_\phi t}}\right]^{2\beta} \tag{56}$$

where

$$\alpha = (1+2\beta)k_\phi \tag{57}$$

When k_ϕ is small, Eq. 56 can be approximated as

$$K/K_o \cong e^{-\alpha t} \tag{58}$$

Substituting Eq. 52 for $m \neq 0$ into Eq. 37 yields

$$\frac{K}{K_o} = (1+\lambda t)^{-\delta}\left[\frac{1-\phi_o}{1-\phi_o(1+\lambda t)^{-1/r}}\right]^{2\beta} \tag{59}$$

where

$$\lambda \equiv k_\phi \phi_o^r \tag{60}$$

$$\delta \equiv (1+2\beta)/r \tag{61}$$

For short times and/or small k_ϕ, Eq. 59 can be approximated by

$$K/K_o \cong (1+\lambda t)^{-\delta} \tag{62}$$

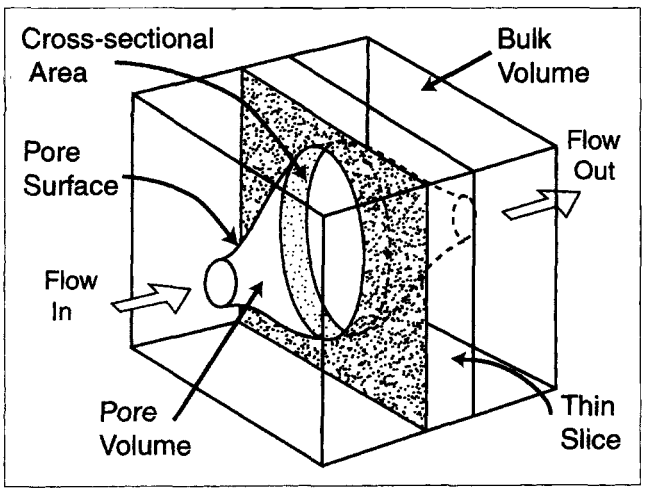

Figure 4. Pore space and thin-slice representations.

For convenience in laboratory measurements by flowing a solution with constant concentration (hence, F_s = constant also), Schechter and Gidley (1969) used cross-sectional area measurements of single pore sizes during surface dissolution in thin porous disks. Therefore, interpretation of their measurements requires an area formulation for thin slices instead of the bulk volume formulation of porous media given above.

The preceding expressions can be applied for a thin slice shown in Figure 4, for which $L_h \cong L_b$, and therefore $\tau \cong 1.0$. Consequently, Eq. 12 becomes

$$\phi = nA_h/A_b \tag{63}$$

Thus, substituting Eq. 63 into Eqs. 37, 50–51, 56, 58, 59 and 62 a thin-section formulation can be obtained as follows. Eq. 37 becomes

$$\frac{KA_{ho}}{K_o A_h} = f(\beta,\gamma)\left[\frac{A_h(A_B-A_{ho})}{A_{ho}(A_B-A_h)}\right]^{2\beta} \tag{64}$$

in which, from Eq. 38

$$f(\beta,\gamma) = \left(\frac{\gamma}{\gamma_o}\right)^2\left(\frac{A_{ho}}{A_B-A_{ho}}\right)^{2(\beta-\beta_o)} \tag{65}$$

where

$$A_B = A_b/n, \tag{66}$$

For $m = 0$, Eq. 50 becomes

$$A_h/A_{ho} = \exp(-k_\phi t) \tag{67}$$

For $m \neq 0$, Eq. 51 becomes

$$A_h^{-r} - A_{ho}^{-r} = k_A t \tag{68}$$

where

$$k_A = k_\phi/A_B^r \tag{69}$$

Equation 52 becomes

$$A_h/A_{ho} = (1+A_{ho}^r k_A t)^{-1/r} \tag{70}$$

For $m = 0$, Eq. 56 becomes

$$\frac{K}{K_o} \cong e^{-\alpha t}\left[\frac{A_B-A_{ho}}{A_B-A_{ho}e^{-k_\phi t}}\right]^{2\beta} \tag{71}$$

For small k_ϕ and/or short time, Eq. 71 simplifies as

$$\frac{K}{K_o} \cong e^{-\alpha t} \tag{72}$$

For $m \neq 0$, Eq. 59 becomes

$$\frac{K}{K_o} \cong (1+\lambda t)^{-\delta}\left[\frac{A_B - A_{ho}}{A_B - A_{ho}(1+\lambda t)^{-1/r}}\right]^{2\beta} \quad (73)$$

Equation 62 is used for short time and/or small k_ϕ (or λ) as

$$K/K_o \cong (1+\lambda t)^{-\delta} \quad (74)$$

Applications and Validation

Carnahan (1990) simulated the variation of porosity by scale precipitation at constant temperature and also under constant temperature gradient in a 5-m-long porous medium using a reactive chemical transport simulator. For the isothermal precipitation example, Carnahan (1990) simulated the precipitation of gypsum at 25°C according to the reaction given by Eq. 39 by injecting 10^{-3} mol/m^2·s $Ca^{2+}_{(aq)}$ and 10^{-3} mol/m^2·s $SO^{2-}_{4(aq)}$ at the inlet of the porous medium. For the nonisothermal precipitation example, Carnahan (1990) simulated the precipitation of quartz under a -20°C/m temperature gradient, cooling from 150°C to 50°C over 5 m distance along the porous medium according to Eq. 40 by injecting 10^{-4}mol/m^2·s $Si(OH)^\circ_{4(aq)}$ at the inlet of the porous medium. Carnahan (1990) calculated the porosity variation at the inlet, where the porosity variation was maximum, and temperature and saturation remained constant at 25°C for gypsum and 150°C for quartz precipitation. It should be emphasized that, although the temperature and saturation conditions varied along the porous medium for the nonisothermal case, the temperature and saturation conditions nevertheless remained constant at the inlet face of the porous medium, and are the same of the injected solution entering the medium. Therefore, only the porosity variation at the inlet side of the porous medium occurs under constant temperature and saturation conditions, and has been used to verify the analytic expressions obtained here for F_s = constant. Figure 5 shows the straight-line correlations of Carnahan's (1990) Figures 3 and 6 simulated data of porosity variations by gypsum and quartz precipitation according to Eq. 51. Equation 51 correlates the data with the least-squares linear regression coefficients of $R^2 = 0.9936$ and $R^2 = 0.9979$ for gypsum and quartz, respectively, very close to one, indicating that Eq. 51 can satisfactorily represent the porosity variation by scale precipitation. The best correlation of the porosity variation by the gypsum and quartz precipitations are obtained, respectively, as

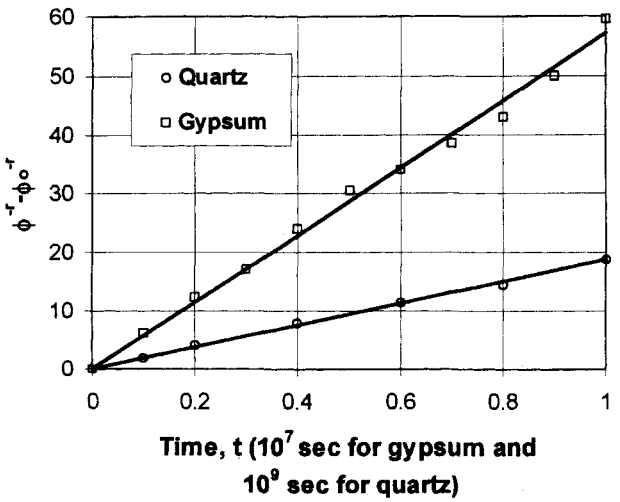

Figure 5. Straight-line plots of Carnahan (1990) simulated data of porosity variation by gypsum and quartz precipitations.

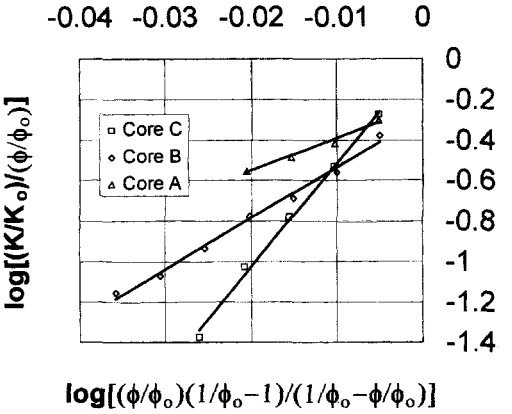

Figure 6. Straight-line plots of permeability vs. porosity data of Bertero et al. (1998) by Civan (1996) power-law flow units equation.

$$\phi^{-r} = \phi_o^{-r} + k_\phi t, \text{at } T = 25^\circ\text{C}, \phi_o = 0.05, r = 0.81, k_\phi = 5.7\times10^{-6}\,\text{s}^{-1}, \text{gypsum} \quad (75)$$

$$\phi^{-r} = \phi_o^{-r} + k_\phi t, \text{at } 150^\circ\text{C}, \phi_o = 0.05, r = 0.81, k_\phi = 1.88\times10^{-8}s^{-1}, \text{quartz} \quad (76)$$

Bertero et al. (1988) measured the permeability reduction caused by scale formation during the simultaneous injection of two incompatible brine solutions into porous rock core samples. They determined the amounts of scales formed in the cores by weighting the cores at various times during the experiments. Bertero et al.'s Figure A-2 presents the measured permeability as percentage of the initial permeability vs. the scale volume as percentage of the initial pore volume for three core tests, identified as Cores A, B, and C, in the form of smooth curves. However, they do not report the actual values of the measured data points. In order to construct straight-line plots according to Eq. 37, these curves had to be discretized to generate a set of point readings of the scale quantities at 1% scale volume intervals and the instantaneous permeability and porosity values were calculated using the reported initial porosity and permeability values of 13.9% and 3.8 md for Core A, 12.6% and 45.6 md for Core B, and 15.0% and 262.0 md for Core C. Note that 1 md (milli Darcy) $\cong 10^{-15}$m^2. The instantaneous porosity was calculated by Eq. 55. Figure 6 shows the best straight-line plots of the Cores A, B, and C data according to Eq. 37. The coefficients of the least-squares linear regressions were obtained as $R^2 = 0.9817$, 0.9915, and 0.9958 for Cores A, B, and C, respectively, very

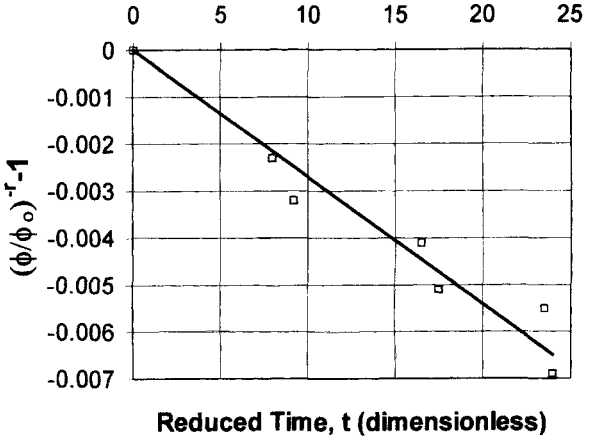

Figure 7. Straight-line plot of Glover and Guin (1973) data of porosity variation by acid dissolution.

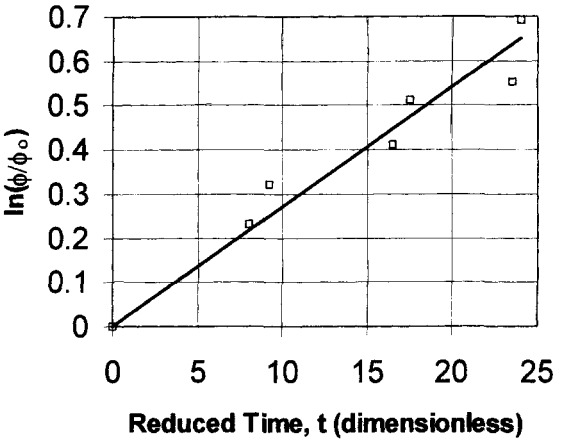

Figure 8. Straight-line plot of Glover and Guin (1973) data of porosity variation by acid dissolution.

close to 1.0, indicate that Eq. 37 accurately represents the permeability-porosity relationship during scale formation. The best permeability-porosity correlations for cores A, B, and C were obtained, respectively, as

$$\frac{K}{K_o} = f_\infty \frac{\phi}{\phi_o}\left[\frac{\phi(1-\phi_o)}{\phi_o(1-\phi)}\right]^{2\beta}, K_o = 3.8md, \phi_o = 0.139,$$

$$\beta = 8.078, f_\infty = 0.59, \text{Core } A \quad (77)$$

$$\frac{K}{K_o} = f_\infty \frac{\phi}{\phi_o}\left[\frac{\phi(1-\phi_o)}{\phi_o(1-\phi)}\right]^{2\beta}, K_o = 45.6md, \phi_o = 0.126,$$

$$\beta = 12.55, f_\infty = 0.52, \text{Core } B \quad (78)$$

$$\frac{K}{K_o} = f_\infty \frac{\phi}{\phi_o}\left[\frac{\phi(1-\phi_o)}{\phi_o(1-\phi)}\right]^{2\beta}, K_o = 262md, \phi_o = 0.15,$$

$$\beta = 25.65, f_\infty = 1.0, \text{Core } C \quad (79)$$

Glover and Guin (1973) measured the permeability and porosity enhancement during acid dissolution of porous media. They injected a dilute aqueous *HF* acid solution into Pyrex774 (81% SiO_2) sintered porous glass disks. They monitored the pressure drop across the disk to determine the permeability and measured the porosity of the disks at various time intervals. They report that determination of the initial porosity may have introduced small error. Here, the $\phi_0 = 0.29$ average value of the initial porosity of the four disks was used. Figure 7 presents a straight-line plot of their Figure 4 measured porosity versus reduced time data for all disks according to Eq. 51. The best fit was obtained with a coefficient of the least-squares linear regression of $R^2 = 0.9464$. The best porosity versus time correlation was obtained as

$$\phi^{-r} = \phi_o^{-r} + k_\phi t, \phi_o = 0.29, r = 0.01, k_\phi = 3.037\times10^{-4} \quad (80)$$

where t is reduced or dimensionless. Because the value of r is small and r appears in the exponent, the accuracy of k_ϕ obtained by Eq. 80 is expected to be low. Because $r \cong 0$ and $m \cong 0$ by Eq. 47, the best straight-line plot of the same data according to Eq. 50 is given in Figure 8. The best least-squares linear fit of the data was obtained as follows with a coefficient of regression of $R^2 = 0.9465$

$$\phi/\phi_o = \exp(k_\phi t), k_\phi = 2.71\times10^{-2} \quad (81)$$

where t is reduced or dimensionless. Thus, Eq. 50 closely represents their Figure 4 experimental data. Because their discrete porosity and permeability enhancement data, reported in their Figures 4 and 5, respectively, have been collected at different time instances, not at the same discrete times, these data have been first smoothed by best curve fitting, and then the discrete values of porosity and permeability corresponding to the same time instances have been sampled at 10 unit intervals of the reduced time and plotted in Figure 9 according to Eq. 37. The best straight-line fit was obtained with a coefficient of the least-squares linear regres-

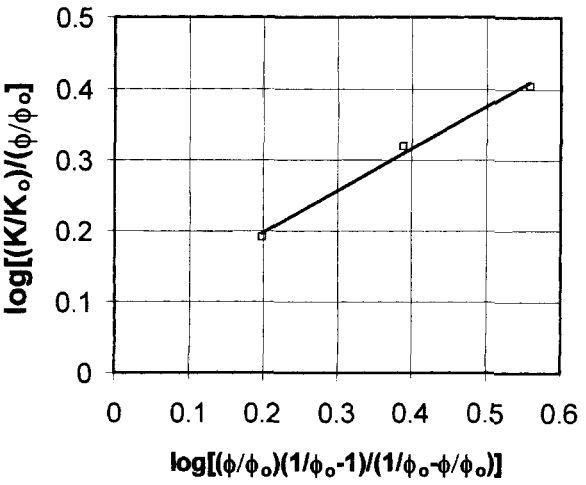

Figure 9. Straight-line plot of permeability vs. porosity of Glvoer and Guin (1973) by Civan (1996) power-law flow units equation.

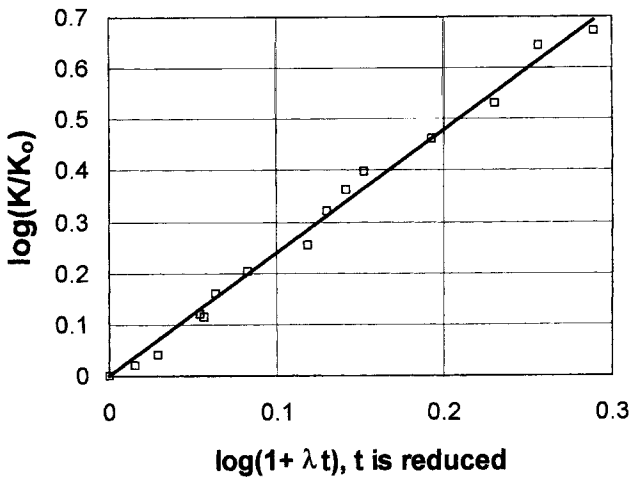

Figure 10. Straight-line plot of Glover and Guin (1973) data of permeability variation by acid dissolution.

sion of $R^2 = 0.992$, indicating that Eq. 37 satisfactorily represents the data. The best porosity-permeability correlation was obtained as

$$\frac{K}{K_o} = f_\infty \frac{\phi}{\phi_o}\left[\frac{\phi(1-\phi_o)}{\phi_o(1-\phi)}\right]^{2\beta}, \phi_o = 0.29, \beta = 0.295, f_\infty = 1.2 \tag{82}$$

Note that Glover and Guin (1973) did not report the initial permeability K_o value and only reported K/K_o. Figure 10 shows a plot of the Glover and Guin (1973) Figure 5 permeability versus reduced time data according to Eq. 62. The least-squares linear fit of the data was obtained with a coefficient of regression of $R^2 = 0.9912$. This indicates that Eq. 62 closely represents the data. The best permeability vs. reduced time correlation was obtained as

$$K/K_o = (1+\lambda t)^{\delta}, \lambda = 3.5\times 10^{-2}, \delta = 2.4 \tag{83}$$

where t is reduced or dimensionless.

Todd and Yuan (1988) only measured the permeability ratio K/K_o in the Clashach sandstone by simultaneous $(Ba, Sr)SO_4$ solid deposition from brines of various concentrations. Their Figure 7 data of Section 1 (injection port) of a test core plug for deposition from brine containing *Sr/Ba* in the ratio of 0.1 is plotted in Figure 11 according to Eq. 62. The best straight-line fit was obtained with a coefficient of regression of $R^2 = 0.998$ of the least-squares linear fit, indicating that Eq. 61 also represents the Todd and Yuan (1988) data accurately. The permeability vs. time correlation is obtained as

$$K/K_o = (1+\lambda t)^{-\delta}, \lambda = 0.11\,\text{min}^{-1}, \delta = 1.33 \tag{84}$$

Schechter and Gidley (1969) measured the pore enlargement and permeability improvement of thin porous disks of an Indiana limestone during wormhole development by exposure to 1% HCl acid at room temperature. Their Figure 5 shows the enlargement of a typical pore area, estimated by means of a microscope, vs. the exposure time. Their Figure 6 shows the permeability enhancement vs. the exposure time during the test. Because they report the measurements of the cross-sectional area of pores in thin-slices of the limestone samples, formed in the shape of wormholes, instead of the porosity of the limestone block, the specifically derived Eqs. 68–70 for cross-sectional area formulation were facilitated in this case. The initial cross-sectional area of the pore has been estimated as $A_{ho} = 0.24\text{mm}^2$ by smoothing their data and extrapolating to the initial time of zero, because their data point indicating the initial pore area somewhat deviates from the general trend of the overall data set and therefore appears to be somewhat inaccurate. Figure 12 shows the best fit of Eq. 68 to their Figure 5 data, with a coefficient of regression of

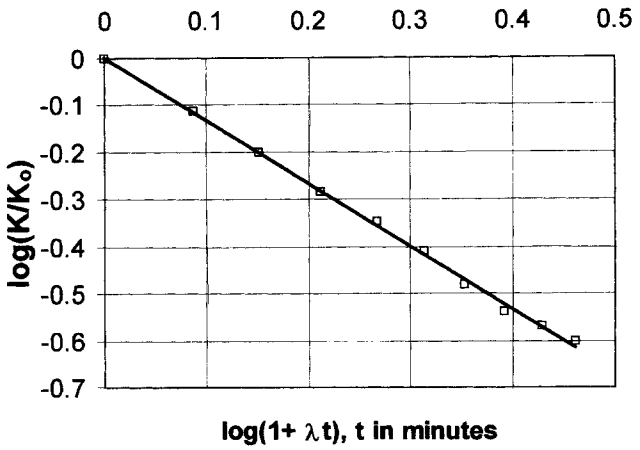

Figure 11. Straight-line plot of Todd and Yuan (1988) data of permeability variation by acid dissolution.

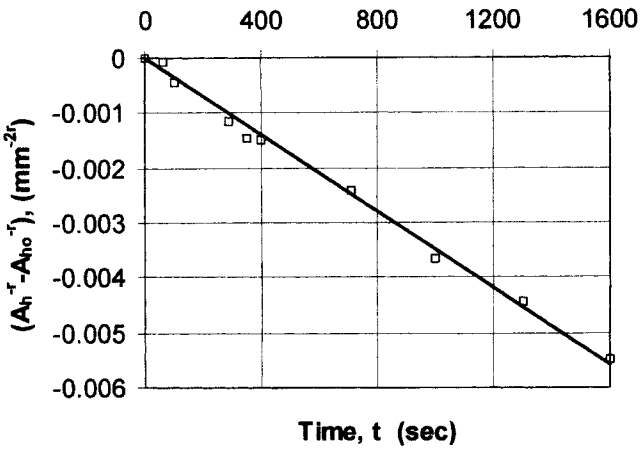

Figure 12. Straight-line plot of Schechter and Gidley (1969) data of pore area variation by acid dissolution.

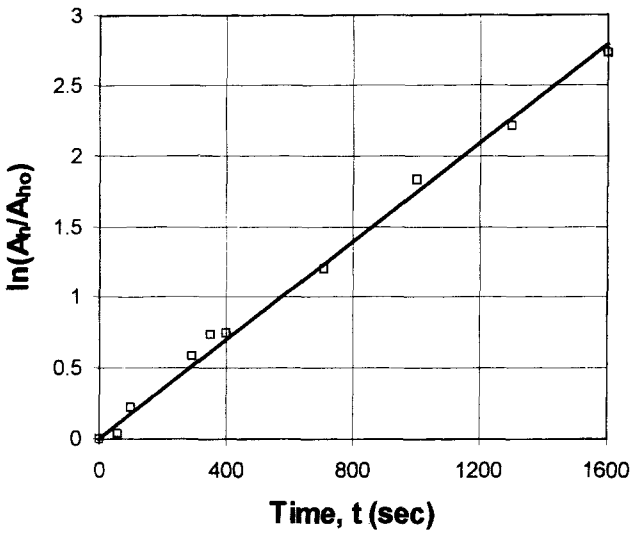

Figure 13. Straight-line plot of Schechter and Gidley (1969) data of pore area variation by acid dissolution.

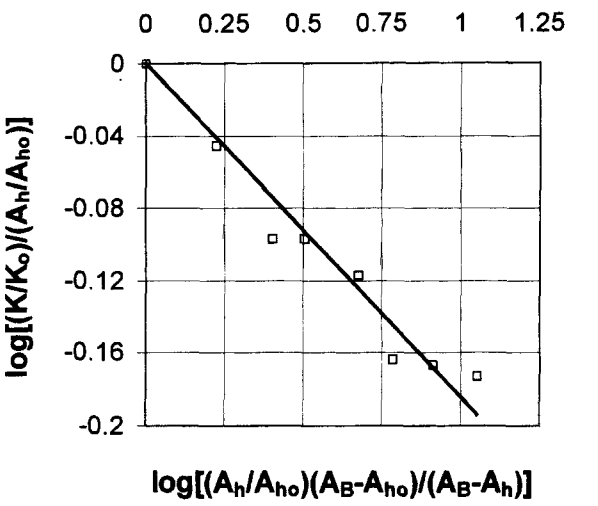

Figure 14. Straight-line plot of permeability vs. porosity data of Schechter and Gidley (1969) by Civan (1996) power-law flow units equation.

$R^2 = 0.9944$. Hence, Eq. 68 satisfactorily represents their Figure 5 data. The best correlation of the pore area vs. time is obtained as

$$A_h^{-r} = A_{ho}^{-r} - k_A t, A_{ho} = 0.24 mm^2, r = 2.0\times10^{-3},$$
$$k_A = 3.0\times10^{-6}\mathrm{s}^{-1} \quad (85)$$

The accuracy of k_A determined by Eq. 85 is suspected to be low because r has a small value and appears in the exponent. Thus, for $r \cong 0$ and $m \cong 0$ by Eq. 47, the value of k_A can be more accurately determined using Eq. 67. The best straight-line fit is obtained as follows with a coefficient of regression of $R^2 = 0.9945$, as shown in Figure 13, when Eq. 67, which assumes $m = 0$, is used

$$\ln(A_h/A_{ho}) = k_\phi t, A_{ho} = 0.24 mm^2, k_\phi = 1.7\times10^{-3}\,\mathrm{s}^{-1} \quad (86)$$

Figure 14 shows the best straightline plot of the Figures 5 and 6 data of Schechter and Gidley (1969) according to Eq. 64. Because they measured the pore cross-sectional area and permeability at different times, both data were first best smooth curve fitted and then the data points were sampled at 200 s time intervals to generate a data set consisting of the discrete point values of the area and permeability at prescribed time instances and used in Figure 14. Their permeability measurement of $K = 32$ md at the 1,600 s time exhibits significantly larger variability, indicating larger measurement errors involved for this measurement. Therefore, this outlier data point was discharged in the straight-line fitting procedure. The remaining eight data points yield the best straight-line fit with a coefficient of regression of $R^2 = 0.9462$, close to one, indicating that Eq. 64 accurately represents all the data points, except for one outlier data point which is suspected of measurement error. The best pore area-permeability correlation is obtained as

$$\frac{K}{K_o} = f_\infty\left(\frac{A_h}{A_{ho}}\right)\left[\frac{A_h(A_B - A_{ho})}{A_{ho}(A_B - A_h)}\right]^{2\beta}, A_B = 30 mm^2,$$
$$A_{ho} = 0.24 mm^2,\ K_o = 2md, \beta = -0.092, f_\infty = 1.0 \quad (87)$$

The minus sign in the beta value indicates $K > K_o$ for scale dissolution. Note that the representative bulk area involving the pore area investigated by Schechter and Gidley (1969) was not reported and therefore had to be estimated as $A_B = 30\mathrm{mm}^2$ by the best fit of Eq. 64 to the data.

Figure 15 shows the plot of the Schechter and Cidley (1969) permeability vs. time data according to Eq. 74. The coeffi-

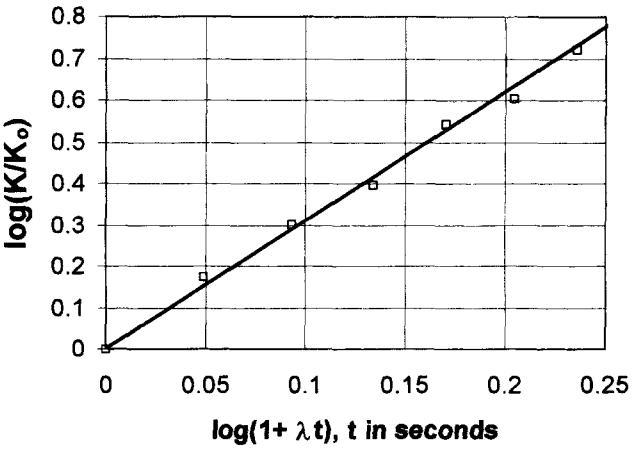

Figure 15. Straight-line plot of Schechter and Gidley (1969) data of permeability variation by acid dissolution.

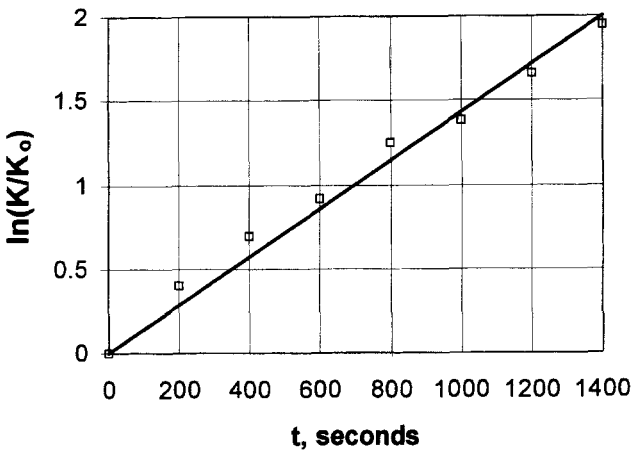

Figure 16. Straight-line plot of Schechter and Gidley (1969) data of permeability variation by acid dissolution.

cient of regression $R^2 = 0.995$, close to one, indicates that Eq. 74 accurately represents their data. The permeability vs. time correlation is obtained as

$$K/K_o = (1+\lambda t)^{\delta},\ K_o = 2md,\ \lambda = 6.0\times10^{-4}\,s^{-1},\ \delta = 3.1 \tag{88}$$

Figure 16 gives the plot of the same data according to Eq. 72 as follows with a coefficient of regression of $R^2 = 0.9824$, lower than that of Eq. 74, but still sufficiently high for practical applications.

$$K/K_o = \exp(\alpha t),\ K_o = 2md,\ \alpha = 1.4\times10^{-3}\,s^{-1} \tag{89}$$

Discussion

The values of the β exponent determined by Eq. 34 are significantly different than the unit value indicated by the Kozeny-Carman equation, (Eq. 1). This should not be surprising because there is ample evidence of this fact in the literature. However, many studies correlated experimental data by the power-law function of porosity instead of the pore-to-matrix volume ration according to

$$K \sim \phi^b \quad \text{or} \quad K/K_o = (\phi/\phi_o)^b \tag{90}$$

where b is an empirical exponent. For example, Reis and Acock (1994) reported 3.05 and 7.33 for Fontainebleau sandstones, and 5.5 for unconsolidated beds for the b exponent. For silica deposition in diatomite, Koh et al. (1996) determined $b = 9.0$, and Bhat and Kovscek (1999) report values in the range of $8.0 \le b \le 9.0$. For paraffin deposition in reservoirs, Ring et al. (1994) found $b = 8.0$. For fluvial/deltaic sandstones, Luffel et al. (1989) obtained

$$K = 6.47\times10^{7}\phi^{8.03} \tag{91}$$

where K is in md and ϕ is a fraction. Lucia (1995) reports the following correlations for three ranges of permeability in sedimentary formations

$$K = 2.884\times10^{3}\phi^{4.275},\ K < 20\ md \tag{92}$$

$$K = 2.040\times10^{6}\phi^{6.38},\ 20 < K < 100\ md \tag{93}$$

$$K = 4.535\times10^{9}\phi^{8.537},\ K > 100\ md \tag{94}$$

Reis and Acock (1994) propose that the exponent values should be even greater than the reported values when permeability measurements are corrected for the Klinkenberg effect. These are only a few but strong indications of high orders of magnitude of the exponent values with respect to ϕ. In the present study, the analyses of experimental data have been carried out with respect to the pore-to-matrix volume ration $\phi/(1-\phi)$. Thus, as indicated by the results presented in the applications section, the absolute values of the exponent of $\phi/(1-\phi)$ vary from values less than $\beta = 1$ to values greater than $\beta = 1$ of the Kozeny-Carman equation. For the specific set of experimental data analyzed here, the smallest value was obtained as $\beta = 0.092$ and the highest value was obtained as $\beta = 25.65$. Based on the theoretical model presented in this article, these values are not surprising. In fact, the theoretical lower limit of $\beta = 0$ can be readily proven if the fractal dimension is set as $\mathfrak{D} = 0$ in Eq. 31. The theoretical upper limit is obtained as $\beta \to \infty$ as $D/\mathfrak{D} \to 1$ in Eq. 31. Obviously, substituting the Euclidean dimension of $D = 2$ yields a value of β in between these limits, that is, $\beta = 1.5$ for $\mathfrak{D} = 3$ according to Eq. 31. An examination of the trends in the analysis of experimental data presented in the applications section implies that the exponent β is a strong inverse function of the porosity ϕ. Therefore, it is reasonable to assume a power-law relationship as

$$\beta^{-1} = C_1\phi^{C_2} \tag{95}$$

where C_1 and C_2 are some empirical parameters. Civan (2000b) also correlated the γ parameter by the Ridgway and Tarbuck (1967) data using Eq. 6, which is similar to Eq. 95. However, as demonstrated by Civan (2000b), the γ and β parameters could also be correlated as functions of the coordination number using Eqs. 4 and 5, because the coordination number is a strong function of porosity in random porous media.

The model presented in this article involves a number of lumped parameters. Specifically, these parameters are: β given by Eq. 35, γ by Eq. 36, r by Eq. 47, k_ϕ by Eq. 48, α by Eq. 57, λ by Eq. 60, and δ by Eq. 61. The basic parameters, such as the dissolution/precipitation rate coefficient and various fractal parameters, have been grouped to derive these parameters. As demonstrated in the applications section by using various data, the best estimates of the lumped parameters can be determined by the least-squares linear fit of the expressions derived for porosity and permeability variation by scales, after these expressions have been rearranged in forms suitable for straight-line plotting. For given fluid and porous materials, laboratory tests can be conducted and the data obtained can be utilized in a similar fashion to determine the best estimates of the lumped parameters for prescribed fluid and porous material systems. This approach is referred to as

the calibration or tuning of the model and is sufficient for many practical applications. However, if also the specific values of the individual basic parameters, including the dissolution/precipitation rate coefficient and the fractal parameters, are being sought, additional data may be required via measurements by appropriate means. For example, the dissolution/precipitation rate coefficient can be measured by various techniques, such as described by Civan (2000c,d). The participating pore surface can be measured by contact angle measurements, such as described by Civan (1997). The parameters of the fractal equation can be determined by a procedure similar to Johns and Gladden (2000). The coordination number and pore surface can be determined by the method of Liu and Seaton (1994). The other basic parameters can also be measured by suitable procedures. However, facilitating the defining expressions of the lumped parameters given in this article may reduce the number of basic parameters to be determined by individual measurements. Although it is feasible to determine the values of all the basic parameters in this way, this tedious task is not warranted and determination of the values of the lumped parameters as described in the applications section, referred to as model calibration procedure, is sufficient for most practical problems. After all, the sole purpose of developing a lumped-parameter model is to avoid such cumbersome measurements. However, it is a comfort to know that the lumped-parameters relate to the basic parameters through the formulation presented in this article.

Although complete formulations for the hydraulic tubes model incorporating fractal dimensions have been presented in this article, the resulting expressions have been simplified and/or analytically solved considering the conditions of usual laboratory tests using core plugs extracted from porous materials. For the purposes of the present study, these simplified expressions have been sufficient. When there are applications to porous media involving varying fluid and flow conditions, the nonsimplified expressions should be used, thus requiring numerical solutions by appropriate numerical methods, well documented in various literature.

Conclusions

The simplified models presented in this article provide insight into the mechanism of porosity and permeability variation in porous media undergoing scale dissolution and precipitation processes and proper means of correlating experimental data with levels of accuracies sufficient for practical applications. The unusually small or large exponents of the pore-to-matrix volume ratio obtained by correlation of empirical data in this study and those reported in the literature compared to the Kozeny-Carman equation have been explained due to the relative fractal dimensions of random porous media. Based on the theory presented in this article, the exponent values may vary in the range of zero to infinity, and therefore significant deviations from the Kozeny-Carman equation, as indicated by correlations of experimental data, are reasonable.

Comparisons with reported data indicate the validity of the considerations and the theoretical derivations presented in this article. It has been demonstrated that the equations derived in this article represent various data accurately with coefficients of regressions very close to one. The simplified models developed in this work may be sufficient and, in fact, preferred for many applications involving porous media to reduce the complexity of the modeling and the computational effort.

The practical and simplified lumped-parameter models presented in this article offer certain advantages. These models lead to simple analytical solutions under laboratory test conditions. The analytical expressions allow for straight-line plotting, practical interpretation, and correlation of experimental data, and a convenient means of validating the proposed models. More importantly, the simplified models derived in this article more accurately represent the experimental data than the previously reported complicated models.

The analytical solutions derived in this article are valid under constant solute saturation conditions of the fluid, and for incompressible and Newtonian fluids, as well as single-phase Darcian flow. When saturation varies, the lumped-parameter model should be solved numerically along with a proper set of equations describing the pore fluid conditions.

Since its inception, the Kozeny-Carman equation has been extensively used for description of the relationship of permeability to porosity and other relevant factors of porous materials. This article demonstrates that it is often useful "to get out of the box," and realize the inherent and long-forgotten assumptions and limitations of the well-accepted theoretical models, such as the Kozeny-Carman equation, which has certainly been an important milestone for characterization of porous materials. Such invaluable theoretical accomplishments may be perceived as guidelines for further potential improvements rather than taking them as granted, including the work presented in this article. In this respect, future studies extending the present formulations for compressible and non-Newtonian fluids, non-Darcian flow, and multiphase fluid systems may be worthwhile. In this article, the improvement of the Kozeny-Carman equation has been theoretically accomplished using the fractal description of the pore attributes. However, because the present derivation is also based on a bundle of hydraulic tubes realization of the porous media fluid flow, its validity is still subject to the inherent limitations of the hydraulic tubes model. Therefore, further modifications for deviations from the hydraulic tubes model may be required and recommended for future work.

Notation

$a_{i,\text{actual}}$ = actual ion activity for species, S_i
$a_{i,\text{equilibrium}}$ = equilibrium saturation ion activity for species, S_i
$\tilde{A}, \tilde{B}, \tilde{A}, \tilde{D}$ = empirical constants, unitless
A_h = surface area of bulk porous media normal to flow, L^2
A_B = bulk area, L^2
A_f = areosity, L^2
A_h = cross-sectional area of hydraulic flow tube, L^2
A_{ho} = reference value of A_h, L^2
A_m = surface area of solid porous matrix normal to flow, L^2
b = empirical exponent, unitless
c = fractal coefficient
C = fractal coefficient
$\mathfrak{C}$ = fractal coefficient
d = fractal dimension
D = fractal dimension
$\mathfrak{D}$ = fractal dimension
D_h = mean hydraulic tube diameter, L
F_s = saturation ratio, unitless

i = index for aqueous species
k = rate coefficient for dissolution or precipitation
k_A = lumped parameter
k_ϕ = lumped parameter
K = permeability, L^2
K_{ap} = actual ion activity product
K_o = reference or base permeability, L^2
K_{sp} = equilibrium saturation ion activity product
L_h = length of tortuous hydraulic flow tube, L
m = exponent of pore surface participation in scale formation or dissolution
M = scale forming mineral
n = number of hydraulic tubes
N = number of aqueous species
p = fluid pressure, $M/L \cdot T^2$
P_h = perimeter of hydraulic tube, L
q = volumetric flow rate through porous media, L^3/T
r = lumped parameter
S_i = aqueous species
t = time, T
V_b = representative elementary bulk volume of porous media, L^3
V_p = pore volume, L^3
Z = coordination number

Greek letters

α = lumped parameter
β = lumped parameter
β_∞ = terminal value of β
δ = lumped parameter
ϵ_s = fractional bulk volume occupied by scales, fraction
ϕ = porosity, fraction
ϕ_o = reference or base porosity, fraction
ϕ_∞ = terminal value of ϕ, fraction
γ = lump parameter
γ_∞ = terminal value of γ
λ = lump parameter
μ = viscosity of fluid, $M/L \cdot T$
σ = fractional pore volume occupied by scales
Σ_b = total pore surface per unit bulk volume, L^2/L^3
Σ_g = specific grain surface per unit bulk volume, L^2/L^3
Σ_p = total pore surface area, L^2
τ = tortuosity, dimensionless
ζ = empirical exponent
ν = exponent
ν_i = stoichiometric coefficient for aqueous species, S_i

Literature Cited

Armaefule, J. O., M. Altunbay, D. Tiab, D. G. Kersey, and D. K. Keelan, "Enhanced Reservoir Description: Using Core and Log Data to Identify Hydraulic (Flow) Units and Predict Permeability in Uncored Intervals/Wells," SPE 26436, *Proc. Ann. Tech. Conf. and Exhibition of the SPE*, Houston, 205 (Oct. 3–6, 1993).

Bertero, L., G. L. Chierici, G. Gottardi, E. Mesini, and G. Mormino, "Chemical Equilibrium Models: Their Use in Simulating the Injection of Incompatible Waters," *SPE Reservoir Eng. J.*, **3**, 288, (Feb. 1988).

Bhat, S. K., and A. R. Kovscek, "Statistical Network Theory of Silica Deposition and Dissolution in Diatomite," *In-Situ*, **23**, 21 (1999).

Brown, G. O., H. T. Hsieh, and D. A. Lucero, "Evaluation of Laboratory Dolomite Core Sample Size Using Representative Elementary Volume Concept," *Water Resources Res.*, **36**, 1199 (2000).

Carman, P. C., "Fluid Flow Through a Granular Bed," *Trans. of Instn. of Chem. Engrs.*, **15**, 150 (1937).

Carman, P. C., "The Determination of the Specific Surfaces of Powders I," *J. Soc. Chem. Ind., London (Trans., Part I)*, **57**, 225 (July 1938).

Carman, P. C., *Flow of Gases Through Porous Media*, Butterworths, London (1956).

Carnahan, C. L., "Coupling of Precipitation-Dissolution Reactions to Mass Diffusion via Porosity Changes," *Chemical Modeling of Aqueous Systems II*, Chap. 18, D. C. Melchior and R. L. Basset, eds., ACS Symp. Ser. 416, 234 (1990).

Chang, F. F., and F. Civan, "Practical Model for Chemically Induced Formation Damage," *J. of Petrol. Sci. and Eng.*, **17**, 123 (1997).

Civan, F., "A Multi-Purpose Formation Damage Model," Paper SPE 31101, *Proc. of SPE Formation Damage Symp.*, Lafayette, LA, p. 311 (1996).

Civan, F., "Model for Interpretation and Correlation of Contact Angle Measurements," *J. of Colloid and Interf. Sci.*, **192**, 500 (1997).

Civan, F., *Reservoir Formation Damage-Fundamentals, Modeling, Assessment, and Mitigation*, Gulf Publ., Houston, (2000a).

Civan, F., "Predictability of Porosity and Permeability Alterations by Geochemical and Geomechanical Rock and Fluid Interactions," Paper SPE 58746, *Proc. of SPE Int. Symp. on Formation Damage,* Lafayette, LA, 359 (Feb. 23–24, 2000b).

Civan, F., "Correlation of the Pit Depth in Crystal Etching by Dissolution," *J. of Colloid and Interface Sci.*, **222**, 156 (2000c).

Civan, F., "Unfrozen Water Content in Freezing and Thawing Soils-Kinetics and Correlation," *J. of Cold Regions Eng.*, **14**, 146 (Sept. 2000d).

De Nevers, N., *Fluid Mechanics*, Addison-Wesley, MA, (1970).

Duda, J. L., "A Random Walk in Porous Media," *Chem. Eng. Ed. J.*, **24**, 136 (Summer, 1990).

Glover, M. C., and J. A. Guin, "Dissolution of a Homogeneous Porous Medium by Surface Reaction," *AIChE J.*, **19**, 1190 (Nov. 1973).

Gruesbeck, C., and R. E. Collins, "Entrainment and Deposition of Fine Particles in Porous Media," *SPEJ*, **22**, 847 (Dec. 1982).

Holstad, A., "Mathematical Modeling of Diagenetic Processes in Sedimentary Basins," *Mathematical Modeling of Flow Through Porous Media*, p. 418, A. P. Bourgeat, C. Carasso, S. Luckhaus, and A. Mikelić, eds., World Scientific Publ., River Edge, NJ (1995).

Honma, S., "A Study of the Seepage Resistance of Suspension-Type Grouts in Soils," *Int. Chem. Eng.*, **33**, 315 (April 1993).

Johns, M. L., and L. F. Gladden, "Probing Ganglia Dissolution and Mobilization in a Water-Saturated Porous Medium using MRI," *J. of Colloid and Interf. Sci.*, **225**, 119 (2000).

Koh, C. J., P. C. Dagenais, D. C. Larson, and A. S. Murer, "Permeability Damage in Diatomite Due to *In-Situ* Silica Dissolution Precipitation," *Proc. of* 1996 *SPE/DOE Tenth Symp. on Improved Oil Recovery*, Tulsa, OK, Paper SPE/DOE 35394, 511 (Apr. 21–24, 1996).

Kozeny, J., "Uber Kapillare Leitung des Wasser im Boden," Sitzungsbericht der Akademie der Wissenschaften, Wien, **136**, 271 (1927).

Le Gallo, Y., O. Bildstein, and E. Brosse, "Coupled Reaction-Flow Modeling of Diagenetic Changes in Reservoir Permeability, Porosity and Mineral Compositions," *J. of Hydrology*, **209**, 366 (1998).

Lichtner, P. C., "Time-Space Continuum Description of Fluid/Rock Interaction in Permeable Media," *Water Resources Res.*, **28**, 3135 (Dec. 1992).

Liu, X., and F. Civan, "Formation Damage and Filter Cake Buildup in Laboratory Core Tests: Modeling and Model-Assisted Analysis," *SPE Formation Evaluation J.*, **11**, 26 (1996).

Liu, S. and J. H. Masliyah, "Single Fluid Flow in Porous Media," *Chem. Eng. Comm.*, **148–150**, 653 (1996).

Liu, X., A. Ormond, K. Bartko, Y. Li, and P. Ortoleva, "A Geochemical Reaction-Transport Simulator for Matrix Acidizing Analysis and Design," *J. of Petroleum Sci. and Eng.*, **17**, 181 (Feb., 1997).

Liu, H., and H. A. Seaton, "Determination of the Connectivity of Porous Solids from Nitrogen Sorption Measurements: III. Solids Containing Large Mesopores," *Chem. Eng. Sci.*, **49**, 1869 (1994).

Lucia, F. J., "Rock-Fabric/Petrophysical Classification of Carbonate Pore Space for Reservoir Characterization," *AAPG Bull.*, **79**, 1275 (Sept., 1995).

Luffel, D. L., W. E. Howard, and E. R. Hunt, "Relationship of Permeability, Porosity, and Overburden Stress Derived From an Extensive Core Analysis Data Base in the Travis Peak Formation," SPE 19008, *Proc. of the SPE Joint Rocky Mountain Regional/Low Permeability Reservoirs Symp. and Exhibition*, Denver, CO, 729 (Mar. 6-8, 1989).

Magnico, P., "Impact of Dynamic Processes on the Coupling Between Fluid Transport and Precipitate Deposition," *Chem. Eng. Sci.*, **55**, 4323 (2000).

Nelson, P. H., "Permeability-Porosity Relationships in Sedimentary Rocks," *The Log-Analyst*, **35**, 38 (May–June 1994).

Nelson, P. H., "Evolution of Peremeability-Porosity Trends in Sandstones," *SPWLA Logging Symp.*, (June 4–7, 2000).

Ochi, J., and J.-F. Vernoux, "Permeability Decrease in Sandstone Reservoirs by Fluid Injection-Hydrodynamic and Chemical Effects," *J. of Hydrology*, **208**, 237 (1998).
Oddo, J. E., and M. B. Tomson, "Why Scale Forms and How to Predict It," *SPE Production & Facilities*, **9**, 47 (Feb. 1994).
Ohen, H. A., and F. Civan, "Simulation of Formation Damage in Petroleum Reservoirs," *SPE Advanced Technology Series*, **1**, 27 (April 1993).
Ortoleva, P., *Geochemical Self-Organization*, Oxford University Press, New York (1994).
Panda, M. N., and W. L. Lake, "Estimation of Single-Phase Permeability from Parameters of Particle-Size Distribution," *AAPG Bulletin*, **78**, 1028 (1994).
Rajani, B. B., "A Simple Model for Describing Variation of Permeability with Porosity for Unconsolidated Sands," *In Situ*, **12**, 209 (1988).
Reis, J. C., and A. M. Acock, "Permeability Reduction Models for the Precipitation of Inorganic Solids in Berea Sandstone," *In Situ*, **18**, 347 (1994).
Revil, A., and L. M. Cathles III, "Permeability of Shaly Sands," *Water Resources Res.*, **35**, 651 (1999).
Ridgway, K., and K. J. Tarbuck, "The Random Packing of Spheres," *British Chemical Engineering*, **12**(3), 384 (1967).
Ring, J. N., R. A. Wattenbarger, J. F. Keating, and S. Peddibhotla, "Simulation of Paraffin Deposition in Reservoirs," *SPE Production & Facilities*, **9**, 36 (Feb. 1994).
Saito, A., S. Okawa, T. Suzuki, and H. Maeda, "Calculation of Permeability of Porous Media Using Direct Simulation Monte Carlo Method (Effect of Porosity and Void Distribution on Permeability)," *Proc. of the ASME/JSME Thermal Eng. Joint Conf.*, L. S. Fletcher, and T. Aihara, (eds)., The American Society of Mechanical Engineers, New York, and The Japan Society of Mechanical Engineers, Tokyo, **3**, 297 (1995).
Schechter, R. S., and and J. L. Gidley, "The Change in Pore Size Distribution from Surface Reactions in Porous Media," *AIChE J.*, **15**(3), 339 (May 1969).
Steefel, C. I., and A. C. Lasaga, "Evolution of Dissolution Patterns-Permeability Change Due to Coupled Flow and Reaction," *Chem. Modeling of Aqueous Systems II*, Chap. 16, p. 212, D. C. Melchior and R. L. Basset (eds.), ACS Symposium Series 416, (1990).
Todd, A. C., and M. D. Yuan, "Barium and Strontium Sulfate Solid Solution Formation in Relation to North Sea Scaling Problems," SPE 18200, *Proc. of Soc. of Petrol. Engs., Ann. Tech. Conf. and Exhibition*, Houston, TX, p. 193 (Oct. 2-5, 1988).
van der Marck, S. C., "Evidence for a Nonzero Transport Threshold in Porous Media," *Water Resour. Res.*, **35**, 595 (1999).
Walsh, M. P., L. W. Lake, and R. S. Schechter, "A Description of Chemical Precipitation Mechanisms and Their Role in Formation Damage During Stimulation by Hydrofluoric Acid," *J. of Petrol. Technol.*, **34**, 2097 (Sept. 1982).

Manuscript received June 21, 1999, and revision received Sept. 5, 2000.